Mechanism of excitonic dephasing in layered InSe crystals

P. Dey,[1] J. Paul,[1] N. Glikin,[1] Z. D. Kovalyuk,[2] Z. R. Kudrynskyi,[2] A. H. Romero,[3] and D. Karaiskaj[1,*]

[1]*Department of Physics, University of South Florida, 4202 East Fowler Avenue, Tampa, Florida 33620, USA*

[2]*Frantsevich Institute of Material Sciences Problems, National Academy of Sciences of Ukraine, Chernivtsi Department, 5 Iryna Vilde Str., 58001 Chernivtsi, Ukraine*

[3]*Physics Department, West Virginia University, Morgantown, West Virginia 26506-6315, USA*

(Received 12 November 2013; revised manuscript received 3 March 2014; published 31 March 2014)

The dephasing and lifetime of excitons in InSe layered crystals are carefully measured using three-pulse, four-wave mixing and two-dimensional Fourier transform (2DFT) spectroscopy. We obtain a detailed picture of the mechanism of excitonic dephasing in this layered material. The 2DFT spectra reveal contributions from the coherent excitation of continuum states, whereas the temperature dependence provides a detailed description of the phonon-exciton interactions and the low temperature limit of the homogeneous linewidth. The excitation density dependence reveals excitation-induced dephasing due to exciton-exciton scattering. The temperature-dependent homogeneous linewidth is dominated by the interaction of excitons with the $\sim$113 cm^{-1} out-of-plane phonon mode.

DOI: 10.1103/PhysRevB.89.125128 PACS number(s): 78.47.jh, 78.47.nj, 78.55.Cr, 78.67.−n

I. INTRODUCTION

The advent of devices based on graphene has generated a wealth of interest in materials that can be made two-dimensional [1]. Graphene exhibits extremely high carrier mobilities but has a vanishingly small band gap, which makes it difficult to use for switching circuits and photodetecting devices. MoS_2 has recently been suggested as an alternative due to its sizable band gap [2,3]. When reduced to a monoatomic layer it exhibits drastic changes in electronic properties. The transition from two atomic layers to a single atomic layer leads to a transformation from an indirect to a direct band-gap semiconductor [4]. Furthermore, single-layer MoS_2 or WSe_2 has intrinsic inversion symmetry breaking, leading to a coupled valley that can be spin polarized with circular polarized light [5–11]. Therefore, it is important to explore new layered materials that could exhibit higher carrier mobilities as well as different band-gap sizes. Group III–VI chalcogenides have exhibited interesting excitonic dynamics, including the non-Markovian memory effects observed in GaSe, resulting from exciton-phonon interactions [12]. However, exciton dynamics in the InSe layered crystal has remained rather unexplored.

The dephasing dynamics exhibited in the coherent response of semiconductors is directly related to both the electronic structure of the excitonic ground state and the many-body interactions taking place. In three-pulse four-wave mixing (FWM), three pulses are incident on the sample, in directions k_a, k_b, and k_c. The nonlinear interaction gives rise to a signal in the direction $-k_a + k_b + k_c$. The phase conjugate pulse $-k_a$ and the second pulse k_b are separated by the time delay τ, whereas the pulse k_b and third pulse k_c are separated by the population time T [Fig. 1(b)]. By varying the time delay τ and monitoring the FWM intensity, referred to as the time-integrated FWM, the dephasing time of excitons can be measured. By varying the time delay T the population relaxation or excitonic lifetime can be measured. In order to monitor the third time evolution t of the FWM signal, additional time-resolved experiments need to be performed.

Recently, greater insight has been obtained by extending the methods of multidimensional Fourier transform spectroscopy into the optical domain. In the present two-dimensional Fourier transform (2DFT) experiments the time delays τ and t are monitored simultaneously and the phase information is preserved. The Fourier transform with respect to these two time delays leads to a 2D map in the frequency domain where the ω_τ and ω_t axes are now correlated. It is the phase preservation throughout the experiment that makes these measurements challenging. However, instrumentation developed recently can overcome these challenges [13,14]. The advantages of multidimensional spectroscopy are well documented in the literature [15]. In semiconductor nanomaterials, 2DFT spectroscopy has allowed accurate measurements of the homogeneous linewidth and provided insights into the microscopic details of many-body interactions [16–19].

In this article we present a series of measurements that provide a detailed picture of the excitonic dynamics in InSe. In particular, we have measured both the excitonic dephasing and the excitonic lifetime on an atomically thin InSe crystal. Detailed temperature- and excitation-density-dependent 2DFT measurements reveal important insights into the dephasing of excitons and many-body interactions taking place.

II. SAMPLE AND EXPERIMENTAL TECHNIQUE

In the present time-resolved study $\sim$130 fs laser pulses at a 76 MHz repetition rate were provided by a standard oscillator. High-quality γ-InSe crystals were grown using the Bridgman method from a nonstoichiometric melt, $In_{1.03}Se_{0.97}$. The crystals were undoped, exhibiting an unintentional n-type conductivity with a majority carrier concentration in the 10^{14} cm^{-3} range. The primitive unit cell of γ-rhombohedral InSe contains three layers, each consisting of four closely packed, covalently bound, monoatomic sheets in the sequence Se-In-In-Se. Within each plane, atoms form hexagons, interacting by weak van der Waals forces among the layers [Fig. 1(c)]. The sample used in the present studies was exfoliated down to submicron

*karaiskaj@usf.edu

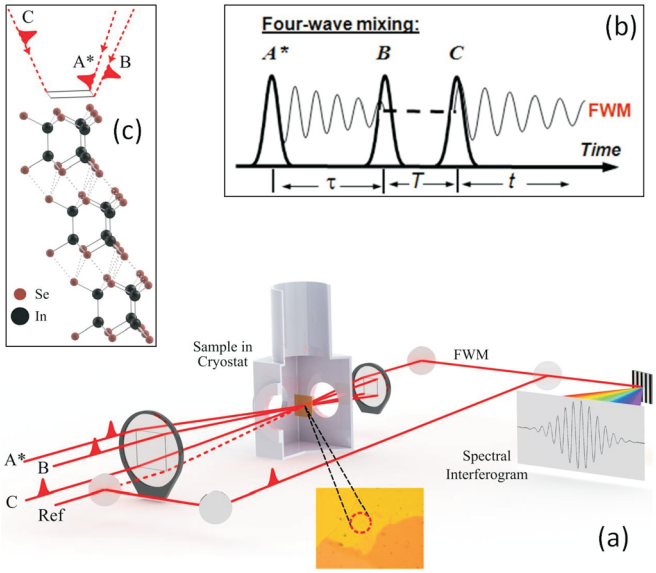

FIG. 1. (Color online) (a) Four-phase stabilized linearly polarized beams obtained from the MONSTR instrument described in Ref. [14] are focused on the sample, which is held in the cryostat at 5 K. A portion of the laser pulse has been split off and colinearly recombined with the FWM signal for heterodyne detection. The combined beams are dispersed in the spectrometer, resulting in the spectral interferogram. (b) The sequence of laser pulses used in the experiments, where A* corresponds to the phase conjugate pulse. The time delay τ corresponds to the time between pulse A* and pulse B, T is the time delay between pulse B and pulse C, and t is the evolution of the FWM in "real time." (c) Crystal structure of γ-rhombohedral InSe, where the unit cell extends over three layers bound through van der Waals interaction along the c axis. The laser excitation shown is perpendicular to the covalently bound layers or parallel to the c axis.

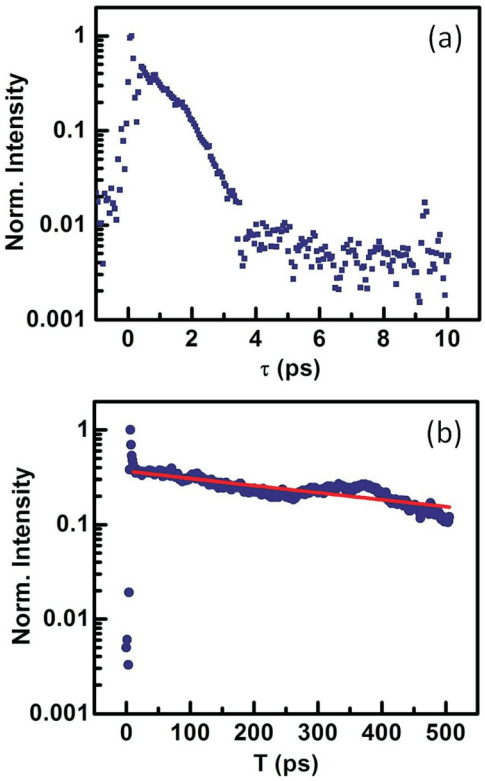

FIG. 2. (Color online) (a) Time-integrated FWM data at 5 K. (b) Population decay of excitons at 5 K. Filled (blue) circles and squares are experimental data, whereas the solid (red) line is the exponential fit, respectively.

thickness. The data were collected from an ∼0.6-μm-thick region shown in Fig. 1(a).

III. RESULTS AND DISCUSSION

Earlier studies have provided details on the electronic properties of this material [20–27]. γ-InSe is a direct band-gap semiconductor with a band gap at the Z point of the Brillouin zone [20]. The electronic band gap has been measured to be 1.352 eV at 10 K and has been shown to become indirect with external pressure [25]. The valence-band maximum is thought to have Γ_1 symmetry, whereas the minimum of the conduction band belongs to Γ_2. The symmetry of the dipole operator for light polarized perpendicular to the c axis belongs to Γ_3, and as a result, the fundamental transition $\Gamma_1 \rightarrow \Gamma_2$ should be dipole forbidden. It only becomes allowed through a weak spin-orbit interaction in the double-group representation, with a relatively low oscillator strength [20]. The low oscillator strength makes time-resolved spectroscopy relying on nonlinear optical effects rather difficult.

Free excitons have been observed in absorption studies with an estimated binding energy of ∼14.5 meV. Despite the strong anisotropy in the effective masses of InSe along and perpendicular to the planes, the energetic position of the exciton levels was well accounted for within the 3D hydrogenic model. The Bohr radius of free excitons was estimated to be 50 Å, which corresponds to a real-space extension over three unit cells of the γ polytype [20,28].

The time-integrated FWM decays as $\exp(-2\tau/T_2)$, where T_2 is the dephasing time and is related to homogeneous linewidth according to $\gamma = 2\hbar/T_2$ [29]. The time-integrated FWM signal was collected at 5 K by scanning τ and the data are shown in Fig. 2(a). An initial rapid decay followed by a rapid recovery has been observed and has been attributed to the destructive interference of the 1s exciton with the continuum states [30,31]. The FWM signal corresponding to the excitonic states was measured at a population time $T = 0$ ps and decayed exponentially with $T_2 \sim 1.4$ ps, comparable to earlier dephasing measurements on GaSe [32]. The excitonic population time T_1 can be obtained by maintaining the time delay τ fixed and varying the delay time T. The intensity vs the time delay T for $\tau = 0$ ps is shown in Fig. 2(b), where the (blue) circles are the experimental data and the solid (red) line is the exponential fit. The single-exponential fit shown corresponds to $T_1 = 1.2$ ns, somewhat larger than previously estimated [33]. Since in this material the dephasing time T_2 is much shorter than the population decay T_1, T_2 provides a good approximation for the pure dephasing time T_2^*. Time-integrated FWM measurements at different T delays were collected but the dephasing time T_2 did not vary, as expected in systems with a long population time.

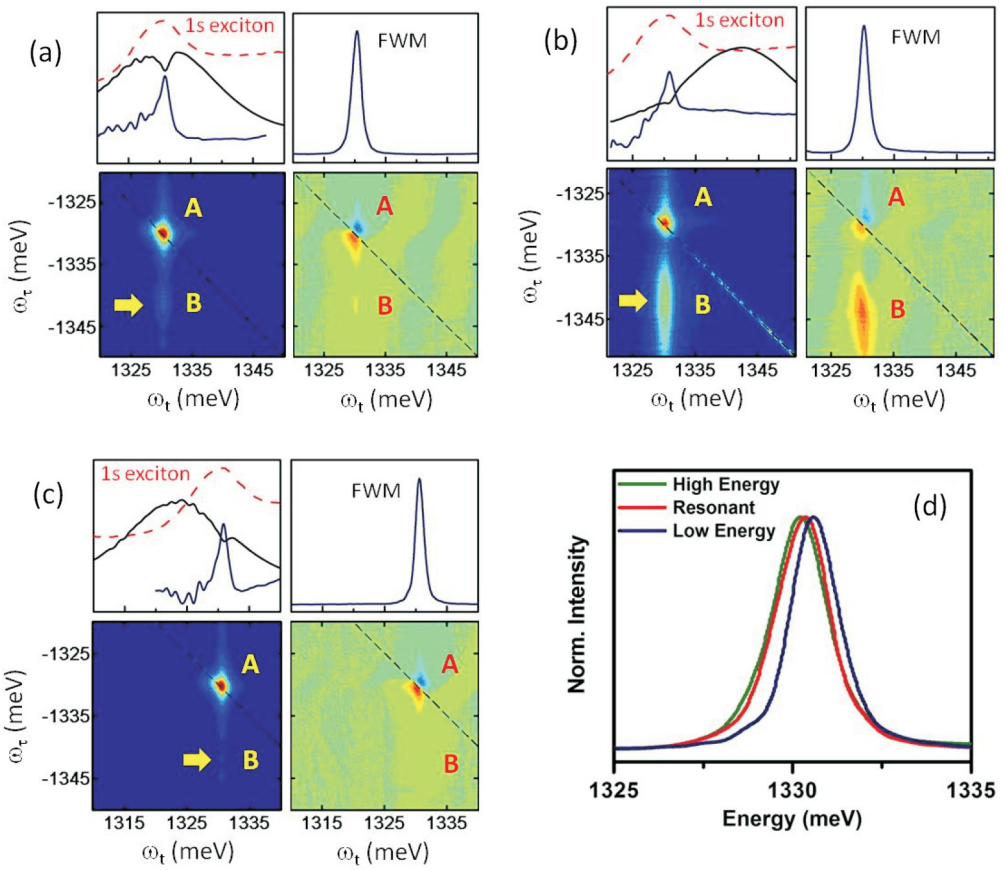

FIG. 3. (Color online) (a–c) 2DFT spectra from the ∼0.6-μm-thick InSe crystal for resonant, high-energy, and low-energy excitation, respectively. Bottom left: Amplitudes. Bottom right: Real part of the complex amplitude. Peak A corresponds to the 1s exciton resonance, whereas peak B is stronger for high-energy excitation. Top left: 1s exciton absorption peak [dashed (red) line] as obtained from the entire sample, 1s exciton peak [solid (blue) line] obtained from the region of the sample where 2DFT experiments were performed, and laser excitation spectra (solid black line). Top right: Corresponding spectrally resolved FWM data. (d) Spectrally resolved FWM for all three excitations are shown together for comparison.

A. 2DFT spectroscopy

2DFT spectroscopy offers a more elegant and direct way of measuring homogeneous broadening. While the profile along the diagonal of the 2DFT spectra marked with a dashed line in Figs. 3(a)–3(a) reflects the inhomogeneous width of the excitonic ensemble, the cross-diagonal profile provides a direct measure of the homogeneous linewidth. Using the method described in Ref. [34] the absolute phase of the signal was obtained and the real parts in Figs. 3(a)–3(c) were retrieved from the complex amplitudes. The projection of the real part of the 2DFT spectra on the ω_t axis was compared with differential absorption data to probe the accuracy of the retrieved phase.

We start the discussion of the 2DFT spectra with Fig. 3(a), where the peak labeled A corresponds to the 1s excitonic resonance, and a weaker elongated peak labeled B appears below the diagonal. In order to further investigate peak B, appearing on the high-energy side of the 2DFT spectra, we center the excitation laser at a higher energy. It should be pointed out that the ω_τ axis is plotted as negative and therefore the higher energy B peak appears below the diagonal. Shifting the laser spectrum farther towards the continuum leads to a strengthening in the intensity of peak B at about half of the 1s excitonic resonance peak A as shown in Fig. 3(b). Peak B disappears almost completely when the laser energy is tuned below the 1s exciton resonance in Fig. 3(c), indicating that peak B likely originates from coherent excitation of continuum states. The emissive line shape in the real part of the 2DFT spectra is also indicative of continuum states. The elongation of the peak B vertically and the appearance below the diagonal are both the result of excitation-induced dephasing [35]. The spectrally resolved FWM is shown in Fig. 3(d) for the three excitation conditions. A small many-body induced renormalization shift toward lower energies can be observed as the excitation energy is shifted toward the continuum [36]. Furthermore, charged carriers are efficient at dephasing excitons. As a result, a modest line broadening is also observed when the continuum states are excited.

B. Homogeneous linewidth temperature dependence

Exciton-phonon interaction can lead to efficient excitonic dephasing and temperature-dependent measurements can be used to probe these interactions. In particular, due to the anisotropic nature of layered crystals the carrier-phonon interactions can lead to peculiar effects. In order to further investigate the effect of phonon scattering on excitonic

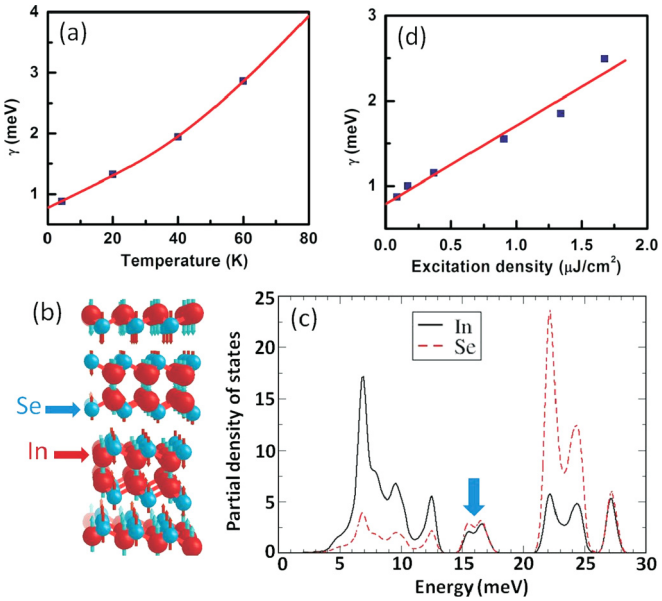

FIG. 4. (Color online) (a) Temperature dependence of the excitonic homogeneous linewidth. Filled (blue) squares are the experimentally measured linewidths, whereas the solid (red) line is the fitting using Eq. (1). (b) The calculated phonon mode corresponding to the out-of-plane vibration, where In and Se atoms vibrate against each other. (c) Partial phonon density of states calculated *ab initio*, showing that the low-frequency phonons originate predominantly from the heavier In atom, whereas the higher frequency phonons originate from the lighter Se atom. Between 14 and 18 meV the contributions to the phonons from both atoms are almost equal. The out-of-plane phonon mode thought to efficiently scatter excitons in InSe is denoted by the (blue) arrow. (d) Excitation density dependence of the homogeneous linewidth. Filled (blue) squares are the experimentally measured linewidths, whereas the solid (red) line is the linear fit.

dephasing, 2DFT spectra as a function of temperature were collected. The homogeneous widths obtained from the cross-diagonal profile of the 2DFT spectra are plotted as a function of temperature in Fig. 4(a). The broadening of excitonic transitions is thought to be caused by acoustic phonon scattering at low temperatures and optical phonons at higher temperatures. Early studies on semiconductor quantum wells concluded that both terms need to be included in the fitting procedure [37]. The elastic acoustic phonon scattering leads to a linear temperature dependence and is given by the first term in Eq. (1), whereas the interaction with optical phonons is proportional to the phonon population of an average optical phonon with frequency Ω. The temperature-independent term γ^* reflects the dephasing caused by the remaining temperature-independent contributions.

The fitting using Eq. (1) reproduces well the experimentally measured linewidths. Absorption measurements on layered InSe crystals observed a strong interaction with a 14-meV phonon, which accounted for the shift of the band-gap energy in the full temperature range between the liquid-helium temperature and 300 K and the temperature broadening of the excitonic lines [20]. The existence of a dominant 14 meV (113 cm^{-1}) phonon mode is clearly supported by our fitting results and is chosen as the average phonon frequency Ω. The fitting shown in Fig. 4(a) leads to $a = 26\ \mu eV/K$. Furthermore, a scattering cross section $b = 6.1$ meV of excitons by optical phonons was also retrieved. Finally, the temperature-independent dephasing leads to the offset of the curve at 0 K and is $\gamma^* \sim 0.8$ meV:

$$\gamma = \gamma^* + aT + \frac{b}{\exp(\hbar\Omega/kT) - 1}. \quad (1)$$

In order to further investigate the predicted phonon mode thought to be the predominant vibration leading to excitonic dephasing, total energy calculations were performed within the framework of the density functional theory and the projector-augmented wave method, as implemented in the Vienna *ab initio* simulation package [38–43]. The calculated partial phonon density of states (DOS) is shown in Fig. 4(c). At energies below 14 meV the contributions to the phonon DOS originate mostly from the In atom, whereas for energies higher than 20 meV most contributions to the phonon DOS originate from the Se atom. In the energy range between 14 and 18 meV, the contributions to the phonon DOS are equally shared between In and Se. It is in this energy region of the phonon DOS that the fitting of the experimental data reveals a strong interaction with a phonon mode. A close examination of the phonon energies at the Γ point reveals a mode at 15.8 meV with an A_1 irreducible representation, which corresponds to the vibration of the In layer moving against the Se layer as shown in Fig. 4(b). At the Γ point no other phonon mode can be found in this energy range, which indicates that this is the only out-of-plane vibration of the In and Se atoms responsible for the observed excitonic dephasing. The energy value obtained from our calculations is in agreement with earlier phonon dispersion calculations and Raman scattering measurements, which have identified the A_1 phonon mode at 115.8 ± 0.6 cm^{-1} [44]. Furthermore, the earlier studies also conclude that for the A_1 mode the layers move against each other in the opposite direction and the displacement vectors of the Se atoms in adjacent planes are out of phase.

C. Excitation-induced dephasing

Another common source of excitonic dephasing at low temperatures is excitation-induced effects, such as exciton-exciton and exciton-carrier scattering [45]. In order to further investigate the role of excitation-induced effects we performed 2DFT experiments over a broad range of excitation powers. Excitation powers from 1.68 all the way to 0.084 $\mu J/cm^2$ per beam were used to excite the sample. A significant reduction in homogeneous linewidth was observed over this excitation range, indicating strong excitation-induced broadening. It was shown early on that excitation-induced dephasing is enhanced as a result of reducing the dimensions in GaAs quantum wells compared to the bulk crystals [46]. Strong exciton-exciton scattering-induced dephasing is common in nanomaterials as a result of the reduced dimensionality and has also been observed in single-walled semiconducting carbon nanotubes [47].

The homogeneous linewidth is measured using the cross-diagonal linewidth of the 2DFT spectra and the obtained linewidths are plotted as a function of excitation density in Fig. 4(d). The data are fitted using the known

linear dependence $\gamma = \gamma^* + \beta n_x$, where γ^* is the density-independent homogeneous width, β is the exciton-exciton and exciton-carrier scattering coefficient, and n_x is the excitation density [29,46,47]. The strong excitation-induced dephasing observed could be the combined effect of predominantly exciton-exciton scattering and, to a lesser extent, scattering by the continuum free carriers. Finally, we obtain a residual excitation density-independent linewidth γ^* of ~0.8 meV.

IV. CONCLUSIONS

In conclusion, we have carefully measured the dephasing of excitons in the layered material InSe. The dephasing time T_2 was measured to be ~1.4 ps. The excitons exhibit the long population lifetime T_1 of 1.2 ns, in agreement with only weakly allowed transitions. Strong excitation-induced dephasing due to exciton-exciton and exciton-carrier scattering was observed. Furthermore, based on the present temperature-dependent 2DFT measurements and previous absorption spectroscopy data, a dominant, likely out-of-plane, 113–116 cm^{-1} phonon mode was identified, which leads to efficient excitonic dephasing. The presence of a phonon mode at this energy is in agreement with previous studies and was confirmed by *ab initio* calculations of the phonon DOS. At the low temperature and low excitation density limit, a residual ~0.8 meV homogeneous linewidth was determined.

ACKNOWLEDGMENTS

P.D., J.P., N.G., and D.K. acknowledge the NSF for financial support. A.H.R. recognizes the support of the Marie Curie Actions from the European Union in the international incoming fellowships (Grant No. PIIFR-GA-2011-911070) and the computer resources provided by RES (Red Española de Supercomputación), the TACC-Texas Supercomputer Center, and MALTA-Cluster.

[1] K. S. Novoselov, A. K. Geim, S. V. Morozov, D. Jiang, Y. Zhang, S. V. Dubonos, I. V. Grigorieva, and A. A. Firsov, Science **306**, 666 (2004).
[2] H. S. Lee, S.-W. Min, Y.-G. Chang, M. K. Park, T. Nam, H. Kim, J. H. Kim, S. Ryu, and S. Im, Nano Lett. **12**, 3695 (2012).
[3] T. Georgiou, R. Jalil, B. D. Belle, L. Britnell, R. V. Gorbachev, S. V. Morozov, Y.-J. Kim, A. Gholinia, S. J. Haigh, O. Makarovsky, L. Eaves, L. A. Ponomarenko, A. K. Geim, K. S. Novoselov, and A. Mishchenko, Nature Nanotechnol. **8**, 100 (2013).
[4] K. F. Mak, C. Lee, J. Hone, J. Shan, and T. F. Heinz, Phys. Rev. Lett. **105**, 136805 (2010).
[5] H. Zeng, J. Dai, W. Yao, D. Xiao, and X. Cui, Nature Nanotechnol. **7**, 490 (2012).
[6] K. F. Mak, K. He, J. Shan, and T. F. Heinz, Nature Nanotechnol. **7**, 494 (2012).
[7] T. Cao, G. Wang, W. Han, H. Ye, C. Zhu, J. Shi, Q. Niu, P. Tan, E. Wang, B. Liu, and J. Feng, Nature Commun. **3**, 887 (2012).
[8] S. Wu, J. S. Ross, G.-B. Liu, G. Aivazian, A. Jones, Z. Fei, W. Zhu, D. Xiao, W. Yao, D. Cobden, and X. Xu, Nature Phys. **9**, 149 (2013).
[9] A. M. Jones, H. Yu, N. J. Ghimire, S. Wu, G. Aivazian, J. S. Ross, B. Zhao, J. Yan, D. G. Mandrus, D. Xiao, W. Yao, and X. Xu, Nature Nanotechnol. **8**, 634 (2013).
[10] K. F. Mak, K. He, C. Lee, G. H. Lee, J. Hone, T. F. Heinz, and J. Shan, Nat. Mater. **12**, 207 (2013).
[11] J. A. Schuller, S. Karaveli, T. Schiros, K. He, S. Yang, I. Kymissis, J. Shan, and R. Zia, Nature Nanotechnol. **8**, 271 (2013).
[12] H. Tahara, Y. Ogawa, and F. Minami, Phys. Rev. Lett. **107**, 037402 (2011).
[13] A. D. Bristow, D. Karaiskaj, X. Dai, T. Zhang, C. Carlsson, K. R. Hagen, R. Jimenez, and S. T. Cundiff, Rev. Sci. Instrum. **80**, 073108 (2009).
[14] P. Dey, J. Paul, J. Bylsma, S. Deminico, and D. Karaiskaj, Rev. Sci. Instrum. **84**, 023107 (2013).
[15] S. T. Cundiff, Opt. Express **16**, 4639 (2008).
[16] D. Karaiskaj, A. D. Bristow, L. Yang, X. Dai, R. P. Mirin, S. Mukamel, and S. T. Cundiff, Phys. Rev. Lett. **104**, 117401 (2010).
[17] K. W. Stone, K. Gundogdu, D. B. Turner, X. Li, S. T. Cundiff, and K. A. Nelson, Science **324**, 1169 (2009).
[18] D. Turner and K. Nelson, Nature **466**, 1089 (2010).
[19] J. Bylsma, P. Dey, J. Paul, S. Hoogland, E. H. Sargent, J. M. Luther, M. C. Beard, and D. Karaiskaj, Phys. Rev. B **86**, 125322 (2012).
[20] J. Camassel, P. Merle, H. Mathieu, and A. Chevy, Phys. Rev. B **17**, 4718 (1978).
[21] A. R. Goñi, A. Cantarero, U. Schwarz, K. Syassen, and A. Chevy, Phys. Rev. B **45**, 4221 (1992).
[22] R. Sporken, R. Hafsi, F. Coletti, J. M. Debever, P. A. Thiry, and A. Chevy, Phys. Rev. B **49**, 11093 (1994).
[23] S. Nüsse, P. H. Bolivar, H. Kurz, F. Levy, A. Chevy, and O. Lang, Phys. Rev. B **55**, 4620 (1997).
[24] F. J. Manjón, A. Segura, V. Muñoz-Sanjosé, G. Tobías, P. Ordejón, and E. Canadell, Phys. Rev. B **70**, 125201 (2004).
[25] D. Errandonea, A. Segura, F. J. Manjón, A. Chevy, E. Machado, G. Tobias, P. Ordejón, and E. Canadell, Phys. Rev. B **71**, 125206 (2005).
[26] D. Errandonea, D. Martínez-García, A. Segura, J. Haines, E. Machado-Charry, E. Canadell, J. C. Chervin, and A. Chevy, Phys. Rev. B **77**, 045208 (2008).
[27] M. Millot, J.-M. Broto, S. George, J. González, and A. Segura, Phys. Rev. B **81**, 205211 (2010).
[28] J. V. McCanny and R. B. Murray, J. Phys. C: Solid State Phys. **10**, 1211 (1977).
[29] J. Shah, *Ultrafast Spectroscopy of Semiconductors and Semiconductor Nanostructures* (Springer-Verlag, Berlin, 1999).
[30] J. Feldmann, T. Meier, G. von Plessen, M. Koch, E. O. Göbel, P. Thomas, G. Bacher, C. Hartmann, H. Schweizer, W. Schäfer, and H. Nickel, Phys. Rev. Lett. **70**, 3027 (1993).
[31] S. T. Cundiff, M. Koch, W. H. Knox, J. Shah, and W. Stolz, Phys. Rev. Lett. **77**, 1107 (1996).

[32] F. Minami, A. Hasegawa, T. Kuroda, and K. Inoue, J. Lumin. **53**, 371 (1992).
[33] J. L. Brebner, T. Steiner, and M. Thewalt, Solid State Commun. **56**, 929 (1985).
[34] A. D. Bristow, D. Karaiskaj, X. Dai, and S. T. Cundiff, Opt. Express **16**, 18017 (2008).
[35] C. N. Borca, T. Zhang, X. Li, and S. T. Cundiff, Chem. Phys. Lett. **416**, 311 (2005).
[36] G. Tränkle, H. Leier, A. Forchel, H. Haug, C. Ell, and G. Weimann, Phys. Rev. Lett. **58**, 419 (1987).
[37] D.-S. Kim, J. Shah, J. E. Cunningham, T. C. Damen, W. Schäfer, M. Hartmann, and S. Schmitt-Rink, Phys. Rev. Lett. **68**, 1006 (1992).
[38] P. E. Blöchl, Phys. Rev. B **50**, 17953 (1994).
[39] G. Kresse and D. Joubert, Phys. Rev. B **59**, 1758 (1999).
[40] G. Kresse and J. Hafner, Phys. Rev. B **47**, 558 (1993).
[41] G. Kresse and J. Hafner, Phys. Rev. B **49**, 14251 (1994).
[42] G. Kresse and J. Furthmüller, Phys. Rev. B **54**, 11169 (1996).
[43] J. P. Perdew, K. Burke, and M. Ernzerhof, Phys. Rev. Lett. **77**, 3865 (1996).
[44] C. Ulrich, M. A. Mroginski, A. R. G. Ni, A. Cantarero, U. Schwarz, V. M. Noz, and K. Syassen, Phys. Status Solidi B **198**, 121 (1996).
[45] L. Schultheis, J. Kuhl, A. Honold, and C. W. Tu, Phys. Rev. Lett. **57**, 1635 (1986).
[46] A. Honold, L. Schultheis, J. Kuhl, and C. W. Tu, Phys. Rev. B **40**, 6442 (1989).
[47] Y.-Z. Ma, M. W. Graham, G. R. Fleming, A. A. Green, and M. C. Hersam, Phys. Rev. Lett. **101**, 217402 (2008).